

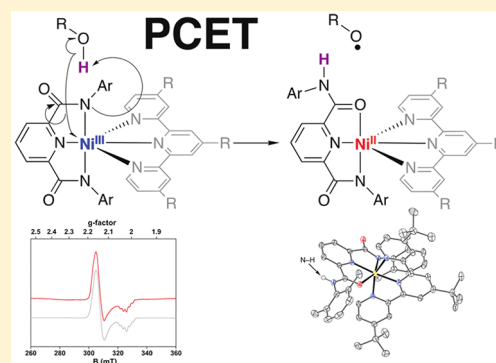
## Carboxamidate Ligand Noninnocence in Proton Coupled Electron Transfer

Caitilín McManus,<sup>‡</sup> Prasenjit Mondal,<sup>‡</sup> Marta Lovisari, Brendan Twamley, and Aidan R. McDonald\*<sup>§</sup>

School of Chemistry, Trinity College Dublin, The University of Dublin, College Green, Dublin 2, Ireland

## Supporting Information

**ABSTRACT:** Recent breakthroughs have brought into question the innocence (or not) of carboxamidate donor ligands in the reactivity of high-valent oxidants. To test the reactivity properties of high-valent carboxamidate complexes,  $[\text{Ni}^{\text{II}}(\text{'Bu-terpy})(\text{L})]$  (**1**,  $\text{'Bu-terpy} = 4,4',4''\text{-tert-butyl-2,2';6',2''-terpyridine}$ ;  $\text{L} = \text{N,N}'\text{-(2,6-dimethylphenyl)-2,6-pyridinedicarboxamidate}$ ) was prepared and converted to  $[\text{Ni}^{\text{III}}(\text{'Bu-terpy})(\text{L})]^+$  (**2**) using ceric ammonium nitrate. **2** was characterized using electronic absorption and electron paramagnetic resonance spectroscopies and electrospray ionization mass spectrometry. **2** was found to be a capable oxidant of phenols and through kinetic analysis was found to oxidize these substrates via a nonconcerted or partially concerted proton coupled electron transfer (PCET) mechanism. The products of PCET oxidation of phenols by **2** were phenoxyl radical and the protonated form of **1**,  $\text{1H}^+$ .  $\text{1H}^+$  was crystallographically characterized providing convincing evidence of **1**'s ability to act as a proton acceptor. We demonstrate that the complex remained intact through a full cycle of oxidation of **1** to **2**, PCET of **2** to yield  $\text{1H}^+$ , and deprotonation of  $\text{1H}^+$  to yield **1** followed by reoxidation of **1** to yield **2**. The N–H bond dissociation energy of the protonated amide in  $\text{1H}^+$  was determined to be 84 kcal/mol. Our findings illuminate the role carboxamidate ligands can play in PCET oxidation.



## INTRODUCTION

The conversion of inert, often saturated, hydrocarbons to high value products relies on our ability to activate strong C–H bonds.<sup>1–7</sup> Enzymes have evolved to employ an array of high-valent transition-metal oxidants that activate strong C–H bonds. Such species have been identified as containing terminal metal-oxo ( $\text{M}=\text{O}$ ) or bridging metal-oxo entities. Great effort has been made to mimic the structural, electronic, and reactivity properties of these metal-based oxidants.<sup>4,7–13</sup> Such complexes are designed to imbue sufficient stability into metastable high-valent oxidants. Supporting ligands are therefore required to be excellent sigma-donors or contain anionic donors to stabilize metals in high oxidation states.

In this regard, anionic carboxamidate supporting ligands have been used with great success because of their ability to stabilize complexes with metals in high oxidation states. Pioneering work by Collins and co-workers has demonstrated the stabilizing effect of anionic tetraamidomacrocyclic ligands (TAMLs) to support  $\text{M}=\text{O}$ 's.<sup>14,15</sup> Borovik and co-workers have similarly employed anionic tris-urea ligands to support a large array of  $\text{M}=\text{O}$ 's.<sup>16–19</sup> Tolman and co-workers have also demonstrated the use of the 2,6-pyridinedicarboxamidate for supporting high-valent Cu complexes.<sup>20–22</sup> We and others found that the same ligand was ideal for trapping high-valent Ni species.<sup>23–30</sup> Most recently, Fukuzumi and co-workers have reported a mononuclear nonheme manganese(III)–aqua complex supported by a carboxamidate ligand that was a capable oxidant.<sup>31</sup> In a similar light, Garcia-Bosch and co-

workers reported another carboxamidate-supported complex that facilitated the oxidation of benzyl alcohol.<sup>32</sup> There is thus a very large cohort of carboxamidate complexes that facilitate biomimetic oxidation reactions.

The high-valent oxidants tend to react with hydrocarbon C–H bonds through a proton coupled electron transfer (PCET) oxidation mechanism. PCET represents a class of C–H oxidation reactions where a proton and electron are transferred in a nonconcerted or concerted fashion.<sup>33–36</sup>  $\text{M}=\text{O}$  complexes, for example, perform hydrogen atom transfer (HAT, a form of concerted PCET) of C–H bonds to yield a one-electron reduced  $\text{M}-\text{O}-\text{H}$  and a carbon-based radical that will rebound to yield a hydroxylated product and a two-electron reduced metal ion. The factors that determine PCET oxidation are the redox potential of the  $\text{M}^n/\text{M}^{n-1}$  couple and the  $\text{pK}_a$  of the proton accepting entity. For high-valent complexes supported by neutral donor ligands (e.g., polypyridine ligands), the O-atom will always be sufficiently basic to act as a proton acceptor. We were interested in exploring the role that significantly more basic anionic donor ligands (e.g., carboxamidate, amide) may play in PCET oxidation. The recent reports by Fukuzumi and co-workers, where a carboxamidate-supported  $\text{Mn}-\text{OH}_2$  complex was surprisingly capable of HAT,<sup>31</sup> Garcia-Bosch and co-workers, where a carboxamidate ligand was postulated to act as a proton

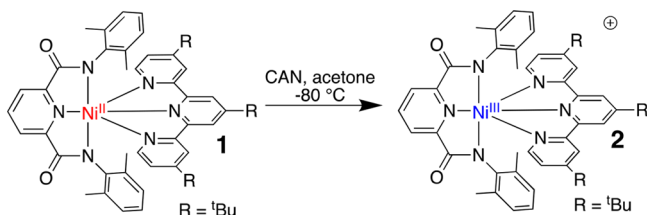
Received: January 10, 2019

acceptor in PCET,<sup>32</sup> and Heyduk and co-workers, who postulated that a diarylamide ligand could act as a H-atom acceptor,<sup>37</sup> heightened this interest. Herein, we explore the role, if any, of the 2,6-pyridinedicarboxamidate ligand in PCET reactions.

## RESULTS AND DISCUSSION

$[\text{Ni}^{\text{II}}(\text{}^t\text{Bu-terpy})(\text{L})]$  (**1**,  $\text{}^t\text{Bu-terpy}$  = 4,4',4''-tri-*tert*-butyl-2,2';6',2''-terpyridine;  $\text{L}$  =  $N,N'$ -(2,6-dimethylphenyl)-2,6-pyridinedicarboxamidate, [Scheme 1](#)) was prepared from

### Scheme 1. Preparation of **2** from **1**<sup>a</sup>



<sup>a</sup>CAN =  $(\text{NH}_4)_2[\text{Ce}^{\text{IV}}(\text{ONO}_2)_6]$ .

$[\text{Ni}^{\text{II}}(\text{NCCH}_3)(\text{L})]$ <sup>26</sup> by ligand exchange with  $\text{}^t\text{Bu-terpy}$  in tetrahydrofuran (THF) (see the [Supporting Information](#) for details). The X-ray structure of **1** demonstrated a  $\text{Ni}^{\text{II}}$  ion in a *pseudo*-octahedral geometry ([Figure 1](#) and [Table S1](#)) and

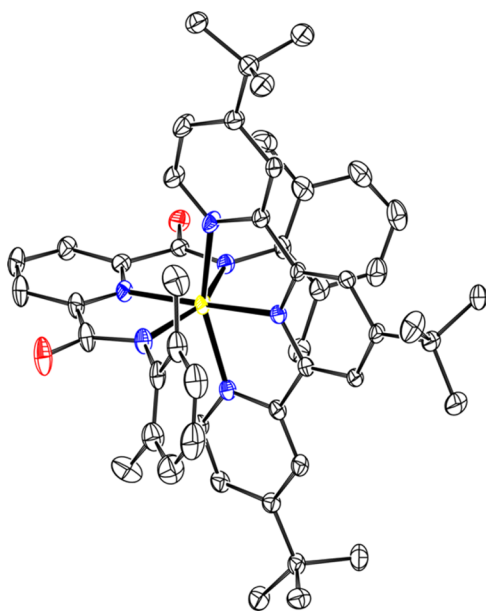


**Figure 1.** ORTEP plot of **1** with atomic displacement shown at 50% probability. Hydrogen atoms and three cocrystallized  $\text{CH}_2\text{Cl}_2$  molecules omitted for clarity.

compared favorably with  $[\text{Ni}^{\text{II}}(\text{terpy})(\text{L})]$  ( $\text{terpy}$  = 2,2';6',2''-terpyridine).<sup>30</sup> The  $^1\text{H}$  nuclear magnetic resonance (NMR) spectrum of **1** showed broad and shifted peaks, consistent with **1** containing a paramagnetic  $\text{Ni}^{\text{II}}$  ion ([Figure S1](#)).<sup>30,38</sup> The number of resonances observed (11) was typical of a symmetric molecule; if there were asymmetry in the molecule, up to 24 resonances would be expected. A magnetic moment ( $\mu_{\text{eff}}$ ) of  $2.51 \mu_{\text{B}}$  was determined using the Evan's method, indicating two unpaired electrons ([Figure S2](#)).<sup>30,38,39</sup> Electro-spray ionization mass spectrometry (ESI-MS) confirmed the

elemental formula of **1** (observed mass =  $831.39 m/z$ ; calculated mass for  $\text{1} + \text{H}^+$  =  $831.39 m/z$ , [Figure S4](#)). We thus determined that complex **1** could be assigned the formula  $[\text{Ni}^{\text{II}}(\text{}^t\text{Bu-terpy})(\text{L})]$  and contained a  $d^8 S = 1 \text{Ni}^{\text{II}}$  ion in a *pseudo*-octahedral ligand field.

The  $\text{Ni}^{\text{II}}$  complex **1** was oxidized to the  $\text{Ni}^{\text{III}}$  complex **2** in acetone at  $-80 \text{ }^\circ\text{C}$  using ceric ammonium nitrate (CAN,  $(\text{NH}_4)_2[\text{Ce}^{\text{IV}}(\text{ONO}_2)_6]$ , 8 equiv, [Scheme 1](#)). The reaction was complete within 400 s. **1** displayed weak features at  $\lambda_{\text{max}} = 420$  and  $840 \text{ nm}$  typical of octahedral  $\text{Ni}^{\text{II}}$  complexes,<sup>30</sup> while **2** demonstrated an intense and broad band at  $\lambda_{\text{max}} = 620 \text{ nm}$  ([Figure 2](#)). Similar features in the visible region have been

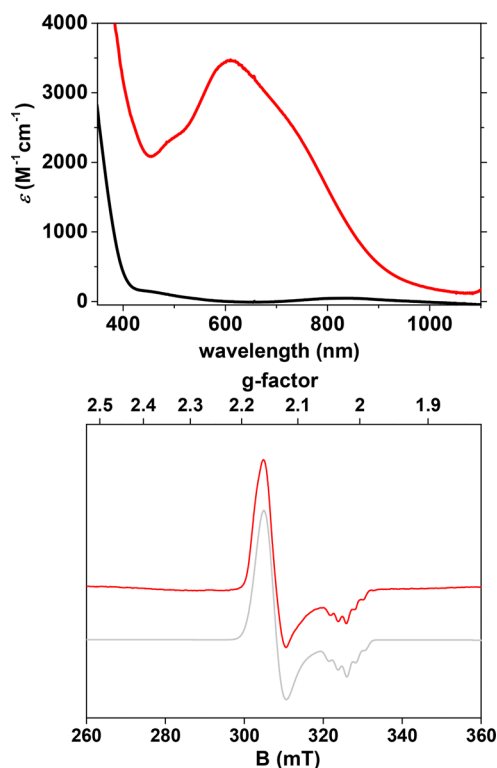


**Figure 2.** (Top) Electronic absorption spectra of **1** (black trace,  $0.4 \text{ mM}$ , acetone) and **2** (red trace, after oxidation of **1** by CAN (8 equiv)) at  $-80 \text{ }^\circ\text{C}$ .  $\epsilon$  calculated on the basis of EPR yield. (Bottom) X-band EPR spectrum of **2** in a frozen acetone solution (red trace) measured at  $77 \text{ K}$ ,  $6.35 \text{ mW}$  microwave power with  $0.3 \text{ mT}$  modulation amplitude, and the simulated spectrum of **2** (gray trace; see the [Supporting Information](#) for simulation details).

reported for octahedral  $\text{Ni}^{\text{III}}$  complexes and analogous  $[\text{Ni}^{\text{III}}(\text{X})(\text{L})]$  complexes.<sup>23–28,30,40,41</sup> **2** could also be generated in the same yield in acetone at  $-80 \text{ }^\circ\text{C}$  using the one-electron oxidant magic blue (*tris*-(4-bromophenyl)ammoniumyl hexachloroantimonate, [Figure S6](#)). ESI-MS of **2** demonstrated a new mass peak at  $m/z = 830.37$  ([Figure S7](#)), which can be attributed to the  $[\text{Ni}^{\text{III}}(\text{}^t\text{Bu-terpy})(\text{L})]^+$  ion. The combined electronic absorption and ESI-MS results led us to assign **2** the formula  $[\text{Ni}^{\text{III}}(\text{}^t\text{Bu-terpy})(\text{L})]^+$ .

Electron paramagnetic resonance (EPR) spectroscopy showed that **2** contained an  $S = 1/2 d^7 \text{Ni}^{\text{III}}$  species.<sup>40,42–44</sup> The EPR spectrum of **2** exhibited axial symmetry, where  $g_{\perp} > g_{\parallel}$  and  $g_{\text{av}} = 2.11$  ([Figure 2](#)), indicating an axially elongated octahedral geometry, with the unpaired spin density localized on the Ni ion. **2** displayed hyperfine coupling of five lines in the  $g_{\parallel}$  component, associated with coupling to two equivalent

<sup>14</sup>N-donor ligands.<sup>30</sup> The EPR signal obtained for **2** was similar to those obtained for all other [Ni<sup>III</sup>(X)(L)] complexes, displaying axial symmetry and hyperfine coupling only in g<sub>||</sub>.<sup>24,26,28,30</sup> The yield of the Ni<sup>III</sup> species **2** was calculated to be 70 ± 20%. The obtained spectrum supported the assignment of **2** as [Ni<sup>III</sup>(<sup>t</sup>Bu-terpy)(L)]<sup>+</sup>.

Complex **2** did not decay over the course of 6 h at −80 °C. At 0 °C, **2** displayed a  $t_{1/2}$  = 2250 s. It was decided to explore the reactivity of **2** at −80 °C to ensure no influence of self-decay on our kinetic analysis. **2** did not react with any hydrocarbons with weak C–H bonds (e.g., cyclohexadiene), unlike previous examples of [Ni<sup>III</sup>(X)(L)].<sup>24,26,28</sup> In contrast, *para*-substituted 2,6-di-*tert*-butylphenol (4-X-2,6-DTBP, X = H, CH<sub>3</sub>, OCH<sub>3</sub>, <sup>t</sup>Bu) and 2,4-DTBP reacted readily with **2**, allowing us to derive mechanistic insights from the kinetic analysis of these reactions (Figures S8–S16). Substrates containing relatively strong O–H bonds such as 4-X-2,6-DTBP (where X = Cl, Br, CN, NO<sub>2</sub>) did not react with **2** when added in 3000-fold excess. Furthermore, TEMPO–H (1-hydroxy-2,2,6,6-tetramethylpiperidine), containing a relatively weak O–H bond, reacted at such a high rate (10 equiv reacted within 2 s, Figure S17) with **2** that accurate kinetic analysis was not possible. This demonstrated that a narrow substrate O–H bond dissociation energy (BDE<sub>O–H</sub>) window existed to explore the reactivity of **2** under the experimental conditions employed.

Upon reaction with 4-H-2,6-DTBP, the rate of decay of the characteristic band of **2** ( $\lambda_{\max}$  = 620 nm) was monitored with time (see Figure 3 for the typical reaction). The decay was fitted as first order to obtain a *pseudo*-first order rate constant ( $k_{\text{obs}}$ ), and a plot of  $k_{\text{obs}}$  against [substrate] gave the second order rate constant for the reaction ( $k_2$ , Figures S10–S16). A  $k_2$  for the reaction between 4-H-2,6-DTBP and **2** of 0.004 M<sup>−1</sup> s<sup>−1</sup> was measured at −80 °C. We also explored the reaction of

**2** with 4-H-2,6-DTBP at −40 °C to allow comparison to previously reported [Ni<sup>III</sup>(X)(L)] complexes (Table 1, Figure

**Table 1.** Phenol BDE<sub>O–H</sub>,  $E_{\text{OX}}$ , and  $k_2$  Values

4-X-2,6-DTBP	BDE (kcal/mol) <sup>46</sup>	$E_{\text{OX}}$ (V) vs Fc/Fc <sup>+</sup> <sup>47,48</sup>	$\sigma_p$ <sup>49</sup>	$k_2$ (M <sup>−1</sup> s <sup>−1</sup> )
OCH <sub>3</sub>	78.3	0.53	−0.78	89.0
CH <sub>3</sub>	81.0	0.90	−0.31	0.195
C(CH <sub>3</sub> ) <sub>3</sub>	81.2	0.93	−0.26	0.165
H	82.1	1.07	0	0.004
2,4-DTBP	82.1			0.542

S15). A  $k_2$  value of 0.06 M<sup>−1</sup> s<sup>−1</sup> for **2** at −40 °C was determined. The post-reaction mixtures for this substrate were analyzed by gas chromatography mass spectrometry (GC-MS), showing peaks corresponding to 3,3',5,5'-tetra-*tert*-butyl-[1,1'-bis(cyclohexane)]-2,2',5,5'-tetraene-4,4'-dione (Figure S8). This product provides a strong indication of PCET by **2**, indicating the formation of a phenoxyl radical that underwent radical–radical coupling. A kinetic isotope effect (KIE) of 2.1 was measured for the reaction between **2** and 4-H/D-2,6-DTBP (Figure S16), which compares favorably to other examples of [Ni<sup>III</sup>(X)(L)] complexes oxidatively activating O–H and C–H bonds.<sup>24,26,28,45</sup> These combined observations suggest the rate-limiting step involved the phenolic O–H hydrogen atom. The products of the reaction suggest the formation of a phenoxyl radical in these reactions, suggesting some form of PCET oxidation by **2**.

The  $k_2$  values determined for the substituted 4-X-2,6-DTBP (X = H, CH<sub>3</sub>, OCH<sub>3</sub>, <sup>t</sup>Bu) that did react with **2** spanned a very wide range (Table 1), with 4-OCH<sub>3</sub>-2,6-DTBP (containing the weakest BDE<sub>O–H</sub>) reacting extremely rapidly, while 4-H-2,6-DTBP (containing the strongest BDE<sub>O–H</sub>) demonstrated relatively slow reactivity. Furthermore, a  $k_2$  of 0.54 M<sup>−1</sup> s<sup>−1</sup> was measured for the reaction between **2** and 2,4-DTBP at −80 °C (Figure 3). This represents a 135-fold enhancement for the sterically less encumbered 2,4-DTBP, with both substrates displaying similar BDE<sub>O–H</sub>.<sup>50</sup> A plot of log( $k_2$ ) against substrate BDE<sub>O–H</sub> of the 4-X-2,6-DTBP showed a linear relationship with a negative slope (Figure 4, Table 1). When Gibbs free energies from the  $k_2$  values were derived using the Eyring equation, a  $\Delta G^\ddagger/\Delta(\text{BDE})$  value of 0.99 was obtained (Figure S18). A linear Hammett plot was also produced from this data (Figure 4), demonstrating a large and negative slope of  $\rho = -5.5$ . A plot of  $(RT/F)\ln(k_2)$  against  $E_{\text{OX}}$  ( $R$  = gas constant,  $T$  = temperature,  $F$  = Faraday constant) was also linear with a negative slope value of −0.29 (Figure 4).

**Discussion on Reactivity Properties and Exploration of Mechanism.** In order to put the reactivity of **2** into context, we explored the reaction of **2** with 2,6-DTBP at −40 °C to compare it to previously reported [Ni<sup>III</sup>(X)(L)] (Table 2:  $k_2$  = 0.06 M<sup>−1</sup> s<sup>−1</sup> for **2** at −40 °C;  $k_2$  = 0.13–1.96 M<sup>−1</sup> s<sup>−1</sup> for [Ni<sup>III</sup>(X)(L)] at −40 °C). The rate at which **2** reacted would indicate that introducing a neutral donor (<sup>t</sup>Bu-terpy), unable to act as a H<sup>+</sup>-acceptor, inhibited its reactivity relative to the previously reported [Ni<sup>III</sup>(X)(L)] complexes that had anionic H<sup>+</sup>-accepting ancillary donors (<sup>−</sup>Cl, <sup>−</sup>OAc, <sup>−</sup>ONO<sub>2</sub>). Furthermore, at −40 °C, **2** was unreactive to hydrocarbons with weak C–H bonds (e.g., 9,10-dihydroanthracene, 1,4-cyclohexadiene), whereas the other [Ni<sup>III</sup>(X)(L)] (X = Cl, OAc) were capable of oxidizing such substrates. This demonstrates a marked difference in reactivity properties for

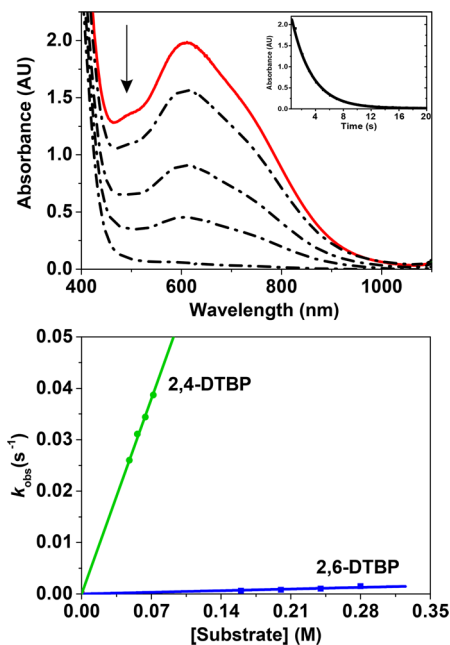


**Figure 3.** (Top) Electronic absorption spectra demonstrating the decay of **2** (red trace) over time upon reaction between **2** and 2,4-DTBP (inset depicts decay of  $\lambda_{\max}$  = 620 nm feature against time). (Bottom) Plot of observed rate versus substrate concentration for the reaction of **2** with 2,4-DTBP (green) and 2,6-DTBP (blue).

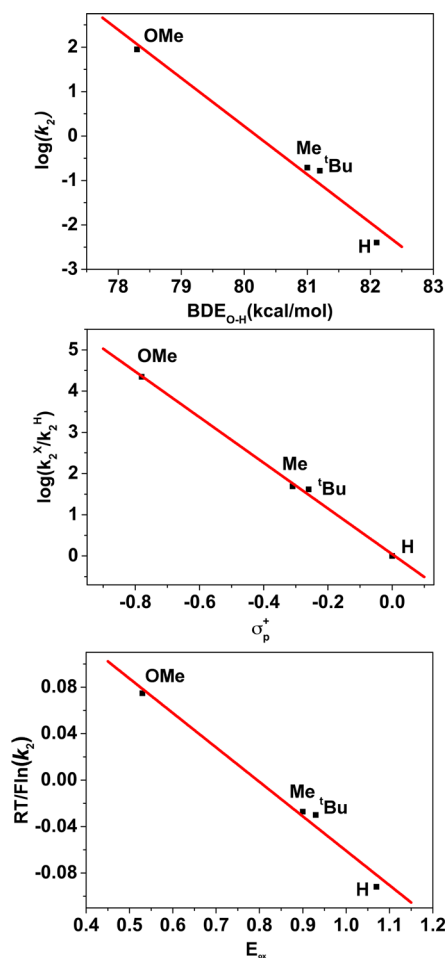


**Figure 4.** Kinetic data for the reaction between **2** and 4-X-2,6-DTBP substrates in acetone. (Top) Plot of  $\log(k_2)$  versus substrate  $BDE_{O-H}$ . (Middle) Hammett plot, slope =  $-5.5$ . (Bottom) Plot of  $(RT/F)\ln(k_2)$  against substrate  $E_{OX}$ , slope =  $-0.29$ . Note: for *p*-Cl/Br/CN/ $NO_2$ -2,6-DTBP, there was no reaction with **2**, whereas for TEMPO-H, very high rates prevented accurate determination of  $k_2$ .

**Table 2.** Phenol  $BDE_{O-H}$ ,  $E_{OX}$ ,  $\sigma_p^+$  Values and  $k_2$  for Their Reaction With **2**<sup>a</sup>

$[Ni(X)(L)]^{+/0}$	$k_2$ ( $M^{-1}s^{-1}$ ) <sup>b</sup>	KIE <sup>c</sup>	$\Delta G^\ddagger/\Delta(BDE)$	$(RT/F)\ln(k_2)/E_{OX}$	ref.
<b>2</b>	0.06	2.1 <sup>d</sup>	0.99 <sup>d</sup>	$-0.29$ <sup>d</sup>	this work
Cl	0.18	2.4 <sup>e</sup>	0.66 <sup>e</sup>	$-0.15$ <sup>e</sup>	28
$O_2CCH_3$	0.13	2.1 <sup>e</sup>	0.31 <sup>f</sup>		26
$ONO_2$	1.96				26

<sup>a</sup>All reactions performed in acetone. <sup>b</sup>Oxidation of 2,6-DTBP at  $-40$  °C. <sup>c</sup>For oxidation of H- or D-2,6-DTBP. <sup>d</sup>Measured at  $-80$  °C. <sup>e</sup>Measured at  $-40$  °C. <sup>f</sup>Determined for C-H bond activation at  $25$  °C.

**2**: **2** was unable to activate weak C-H bonds, thus rendering it thermodynamically less reactive than previous examples of  $[Ni(X)(L)]$  complexes where X was an anionic donor; **2** was also a kinetically less reactive oxidant of phenols than those complexes with anionic ancillary ligands. Thus, although **2** was a capable oxidant, it should be emphasized that it was thermodynamically and kinetically less reactive than analogous complexes with ancillary proton acceptors.

**2** reacted with 2,4- and 2,6-DTBP with a 135-fold enhancement in reactivity for the sterically less encumbered 2,4-DTBP substrate. Such rate enhancement has previously been ascribed to concerted PCET reactions with phenols (HAT), although is considerably higher than previous examples (values in the range of  $\sim 30-70$ ).<sup>24,26,28,50,51</sup> As described below, the mechanism by which **2** reacted with phenols may be a nonconcerted or partially concerted PCET. The large steric effect observed for these substrates thus could indicate alternative forms of PCET and should not be ascribed simply to concerted PCET. The difference in relative rates could also indicate a difference in reaction mechanism between the two substrates, but we have no evidence for such a change. **2** displayed a KIE value of 2.1 for the reactions between **2** and 4-H/D-2,6-DTBP. This compared favorably with many analogous M-O-X oxidants, including all members of the  $[Ni^{III}(X)(L)]$  family, where low KIE values ( $<7$ ) have been observed in the vast majority of cases.<sup>24,26,28,45</sup> This observation simply confirms PCET as rate-limiting but does not provide any insight into whether it was concerted or not.

The large  $\Delta G^\ddagger/\Delta(BDE)$  value (0.99), Hammett  $\rho$ -value ( $-5.5$ ), and the slope of the plot of  $(RT/F)\ln(k_2)$  against substrate  $E_{OX}$  ( $-0.29$ ) all suggested a nonconcerted PCET mechanism or a mechanism where electron transfer (ET) played a greater role in PCET. First, the large  $\Delta G^\ddagger/\Delta(BDE)$  value (0.99) is well in excess of the ideal value predicted by Marcus theory (0.5) and is beyond the range where concerted PCET (HAT) has previously been ascribed (0.15 to 0.7).<sup>34,36</sup> For analogous complexes supported by L, we previously observed  $\Delta G^\ddagger/\Delta(BDE)$  values of 0.31 ( $[Ni^{III}(OAc)(L)]$ , hydrocarbon oxidation) and 0.66 ( $[Ni^{III}(Cl)(L)]$ , phenol oxidation) where concerted PCET (HAT) was implicated in both cases. We conclude that the large  $\Delta G^\ddagger/\Delta(BDE)$  value is indicative of a mechanism of O-H bond activation that does not involve concerted PCET, or involves partially concerted (partial transfer of charge simultaneous with PT), or involves PCET toward different locations (so-called multisite PCET).<sup>52,53</sup>

Second, the slope of the  $(RT/F)\ln(k_2)$  against the substrate  $E_{OX}$  plot ( $-0.29$ ) was higher than would be expected for a concerted PCET reaction. For rate limiting electron transfer (ET), a slope of  $-0.5$  was predicted.<sup>28,54-57</sup> If proton transfer (PT) was rate limiting, this slope would be closer to  $-1.0$ . If the rate determining step was concerted PCET, a slope closer to zero is expected. Our results suggest either concerted PCET or rate-limiting ET for the reaction between **2** and phenols, because the slope was closer to the ideal value for rate-limiting ET. We previously ascribed a slope of  $-0.15$  for  $[Ni^{III}(Cl)(L)]$  to concerted PCET.<sup>28</sup> It is possible that ET was not exclusively rate limiting, with ET and PT demonstrating similar rates. It has previously been suggested that, in cases where the slope is less than  $-0.5$ , a partial transfer of charge may occur in the rate-limiting step.<sup>47,58</sup> It is also possible that multisite PCET, where the proton and electron are delivered to different locations, resulted in intermediary (partially concerted) PCET kinetic behavior.<sup>52,53</sup>

The mechanism by which **2** reacted with phenols appeared to be different from previously reported  $[Ni^{III}(X)(L)]$  oxidants, all of which displayed  $\Delta G^\ddagger/\Delta(BDE)$  values closer to 0.5 and  $(RT/F)\ln(k_2)$  against substrate  $E_{1/2}$  slopes closer to zero, indicating concerted PCET (Tables 1 and 2). In those cases, anionic ancillary ligands were deemed to be acting as proton acceptors forming acetic acid and HCl for  $[Ni^{III}(OAc)-$

(L)] and [Ni<sup>III</sup>(Cl)(L)], respectively. The Ni atom was deemed to be accepting the electron. For **2**, there are multiple plausible proton acceptor groups (carboxamidate O- or N-atoms, pyridine N-atoms) with the Ni atom acting as the likely electron acceptor.

The fact that **2** was capable of oxidizing phenols indicated that the carboxamidate ligand L may be acid/base noninnocent in PCET reactions, with either N- or O-atoms acting as potential H<sup>+</sup>-acceptors. To probe this further, we explored the acid/base chemistry of complexes **1** and **2**. Ni<sup>II</sup> complex **1** did not react with any of the (weakly acidic) 4-X-2,6-DTBP substrates (Figure S19), demonstrating that **2** was the only entity reacting with these phenols. Upon exposure of **1** to two equiv of the more acidic pyridinium triflate (PyHOTf) at -40 °C, a shift in the near-infrared (near-IR) features to lower energy was observed by electronic absorption spectroscopy (Figures 6 and S20, new species defined as **1H**<sup>+</sup>). Such near-IR features have been attributed to a d<sup>8</sup> Ni<sup>II</sup> ion in an octahedral ligand field. The preservation of these features indicated that **1H**<sup>+</sup> maintains an octahedral 6-coordinate environment.<sup>30</sup> The same shift was observed when HCl (one equiv) was used as a H<sup>+</sup>-donor (Figure S21), indicating that the same product was obtained with different H<sup>+</sup>-donors. This would suggest that the protonation reaction does not involve replacement of one of the ligands by <sup>-</sup>OTf (from PyHOTf) or <sup>-</sup>Cl (from HCl).

Satisfyingly, we were able to synthesize and isolate **1H**<sup>+</sup> in the solid state by reacting **1** with two equivalents of pyridinium triflate in CH<sub>2</sub>Cl<sub>2</sub> followed by precipitation with excess THF (see the Supporting Information for details). <sup>1</sup>H NMR analysis comparison of **1** and **1H**<sup>+</sup> showed the conversion of a highly symmetric paramagnetically shifted spectrum for **1** to another paramagnetically shifted spectrum with much lower symmetry for **1H**<sup>+</sup> (Figure S22), indicating monoprotection of the ligand. Fourier transform infrared (FT-IR) analysis of **1H**<sup>+</sup> showed a new feature at  $\nu = 3235\text{ cm}^{-1}$ , which can be ascribed to an N-H vibrational mode (Figure S23). This feature was absent in **1** (Figure S3); however, such N-H resonances were observed in FT-IR spectra of LH<sub>2</sub> (Figure S24). ESI-MS confirmed the elemental formula of **1H**<sup>+</sup> (Figure S25).

Single crystals of **1H**<sup>+</sup> were obtained by slow diffusion of THF into a CH<sub>2</sub>Cl<sub>2</sub> solution of **1H**<sup>+</sup> (Figure 5 and Table S1). **1H**<sup>+</sup> displayed a *pseudo*-octahedral geometry around the Ni<sup>II</sup> center with both pyridine dicarboxamide and <sup>t</sup>Bu-terpy ligands still bound to the Ni<sup>II</sup> ion. However, the binding mode of the

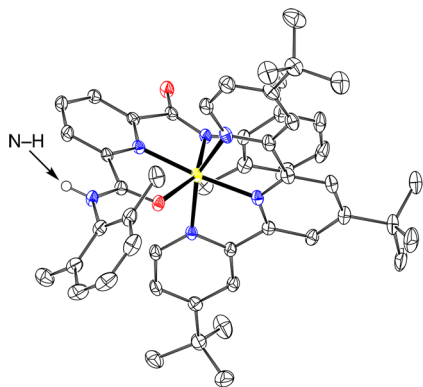


**Figure 5.** ORTEP plot of **1H**<sup>+</sup> with atomic displacement shown at 50% probability. Hydrogen atoms (apart from the amide N-H), trifluoromethane sulfonate counterion, and cocrystallized CH<sub>2</sub>Cl<sub>2</sub> and THF molecules omitted for clarity.

pyridine dicarboxamide was through the central pyridine donor, one carboxamidate N-donor, and one carboxamide O-donor. One of the carboxamidate N-donors was protonated and no longer bound to the metal ion. The C-O and C-N bond lengths of the reconfigured carboxamide were consistent with an amide (1.240(3) and 1.332(3) Å, respectively). A triflate counterion balanced the charge on the complex ion, confirming no change in the overall oxidation state of the complex during protonation. The X-ray crystal structure of **1H**<sup>+</sup> confirmed the H<sup>+</sup>-acceptor capability of the 2,6-pyridinedicarboxamidate ligand in complex **1**.

Critically, the protonation of **1** to yield **1H**<sup>+</sup> was readily reversed by the addition of a slight excess of base (KOH dissolved in CH<sub>3</sub>OH, Figures 6 and S27). We tested the

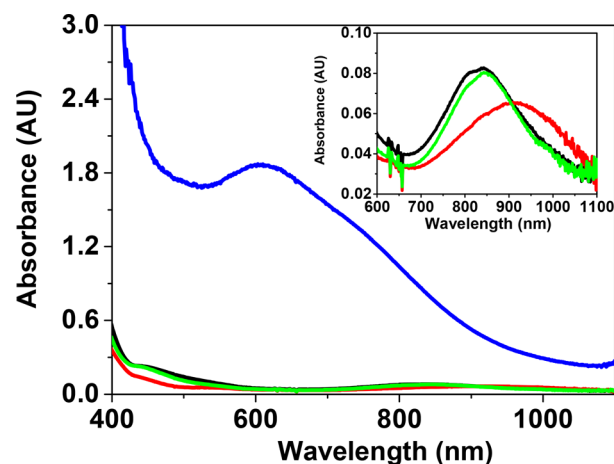


**Figure 6.** Complex **1** (black trace), complex **1H**<sup>+</sup> (red trace, **1** + pyridinium (two equiv)), the reformation of **1** from the reaction between **1H**<sup>+</sup> and KOH (green trace, three equiv KOH), and **2** (blue trace) from the reaction where CAN (8 equiv) was added to the **1** + pyridinium + KOH mixture.

reactivity of a series of bases toward **1H**<sup>+</sup> in CH<sub>3</sub>CN and found that the following bases reacted with **1H**<sup>+</sup> to yield **1**: potassium *tert*-butoxide, KOH, 1,8-diazabicyclo[5.4.0]undec-7-ene (DBU), triethylamine (NEt<sub>3</sub>), *tert*-butylamine, 4-*N,N*-dimethylaminopyridine (DMAP), benzylamine, and imidazole. The latter five bases reacted slowly with respect to the former three consistent with their relative pK<sub>a</sub> values in CH<sub>3</sub>CN (Table S2). In contrast, the following did not react with **1H**<sup>+</sup>: 2,6-lutidine, aniline, and pyridine. This allowed us to estimate the pK<sub>a</sub> of the proton in **1H**<sup>+</sup> to be 15.00 in CH<sub>3</sub>CN (Table S2). We then proceeded to more accurately measure the equilibrium constant (K<sub>a</sub>) for the reaction **1** + PyHOTf → **1H**<sup>+</sup> + Py in order to accurately determine pK<sub>a</sub> for **1H**<sup>+</sup>. Titration of **1** with PyHOTf showed a linear decay of the electronic absorption features associated with **1** (Figure S28). However, a plot of [1H<sup>+</sup>][Py]/[1] against [PyHOTf] was not linear, and therefore, the slope of the plot and thus K<sub>a</sub> could not be determined (Figure S29; see the Supporting Information for details on calculations). The observed nonlinear plot suggests that the reaction between **1** and PyHOTf to yield **1H**<sup>+</sup> was not a simple A-to-B conversion. An isosbestic point was not observed during the titration, confirming that this was not a clean **1** to **1H**<sup>+</sup> conversion (Figure S30). Similar results were obtained for the reverse reaction between **1H**<sup>+</sup> and KOH (Figure S31). This observation is not unexpected given that the N-atom in **1** must undergo protonation, dissociation from

the metal, and rotation around the C<sub>ketone</sub>-N bond (in no particular order) to yield **1H**<sup>+</sup>.

No reaction was observed upon the addition of CAN to **1H**<sup>+</sup>, indicating that **2** could not be generated from **1H**<sup>+</sup>. CV analysis of **1H**<sup>+</sup> demonstrated a chemically irreversible wave at 0.93 V versus Fc/Fc<sup>+</sup> (Figure S26), which is significantly shifted by 0.74 V with respect to **1** (0.19 V versus Fc/Fc<sup>+</sup>, Figure S5). However, **2** was formed in 75% yield when KOH was added to **1H**<sup>+</sup> followed by CAN (Figures 6 and S32). Furthermore, **2** was unreactive toward PyHOTf under the same conditions, showing that it was not capable of acting as a H<sup>+</sup>-acceptor with weak acids. **2** reacted with aqueous HCl yielding a featureless electronic absorption spectrum (Figure S33). Addition of KOH (dissolved in CH<sub>3</sub>OH) resulted in the reformation of **2** (Figure S34). Complex **2** was thus capable of acting as a reversible H<sup>+</sup>-acceptor; however, only very strong acids reacted with **2**, meaning **2** was unlikely capable of deprotonating 4-X-2,6-DTBP substrates.

Once it was established that **1H**<sup>+</sup> was a stable species, it was important to establish its role, if any, in the PCET oxidation of phenols. Analysis of the **2** + 4-OCH<sub>3</sub>-2,6-DTBP post-reaction mixture displayed features that were the same as those obtained for **1H**<sup>+</sup> (Figure 7). In this instance, **1H**<sup>+</sup> was

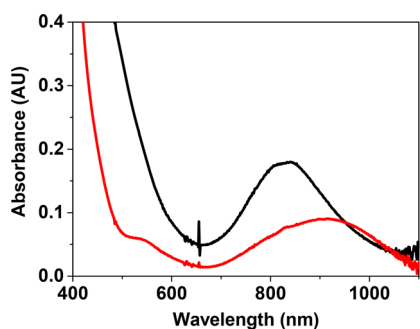


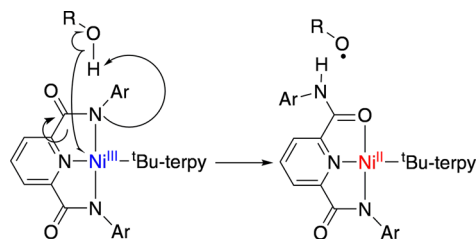
**Figure 7.** Electronic absorption spectrum of the reaction mixture after the reaction between **2** (3 mM) and 4-OCH<sub>3</sub>-2,6-DTBP (red trace, 20 equiv), and that complex **1** (black trace, 3 mM). The red trace is the same as that measured for **1H**<sup>+</sup>.

obtained in 70% yield with respect to **2**, as determined by electronic absorption spectroscopy. The same absorption spectrum was obtained for all other substrates (4-X-2,6-DTBP and TEMPO-H, Figure S35). In these spectra, the characteristic electronic absorption features attributed to **1** were absent. No evidence for Ni<sup>III</sup> (no intense bands in the UV-vis region, EPR silent) was present while <sup>1</sup>H NMR showed only resonances for the substrate (Figure S36). ESI-MS analysis displayed mass ions for **1H**<sup>+</sup>, the substrate, the oxidized product, and fragments of the complex (i.e., {Ni + <sup>t</sup>Bu-terpy}<sup>+</sup>, {Ni + L}<sup>+</sup>, Figure S37). No evidence for oxidative ligand degradation was observed. These observations indicate that **1H**<sup>+</sup> was the sole product of the reaction between **2** and 4-OCH<sub>3</sub>-2,6-DTBP. Addition of KOH to the post-reaction mixture yielded absorption features attributed to **1** (Figure S31), which could in turn be converted back to **2** again by addition of CAN (Figure S32). These observations demonstrate that **1H**<sup>+</sup> was the product of PCET oxidation of 4-X-2,6-DTBP by **2**. Furthermore, it demonstrates that the complex remained intact through a full cycle of oxidation of **1** to **2**, PCET by **2** to yield **1H**<sup>+</sup>, and deprotonation of **1H**<sup>+</sup> to yield **1** followed by reoxidation of **1** to yield **2**.

Our kinetic analysis suggested that **1H**<sup>+</sup> may have reacted through nonconcerted or partially concerted PCET, we therefore decided to assess the driving force for the reaction between **2** and 4-X-2,6-DTBP should the reaction in fact be concerted PCET (homolytic O-H bond cleavage). This can be analyzed by determining the N-H bond dissociation enthalpy (BDE<sub>N-H</sub>) of **1H**<sup>+</sup>. We calculated the BDE<sub>N-H</sub> using methods for metal-based oxidants in PCET pioneered by Mayer and co-workers.<sup>36,53</sup> The following formula was used to calculate BDE: BDE<sub>N-H</sub> = 1.37(pK<sub>a</sub>) + 23.06(E<sub>1/2</sub>) + C<sub>H,CH<sub>3</sub>CN</sub>, yielding a BDE<sub>N-H</sub> for **1H**<sup>+</sup> of ~84 kcal/mol (pK<sub>a</sub> = 15.00; E<sub>1/2</sub> = 0.19 V). The error in this measurement is likely quite high (±3 kcal/mol) given that the pK<sub>a</sub> was estimated as described above. It is important to note that the reactivity studies were performed in acetone while BDE<sub>N-H</sub> was calculated in CH<sub>3</sub>CN because we could not determine the Ni<sup>II/III</sup> E<sub>1/2</sub> accurately in acetone. Furthermore, the nonlinear behavior observed for the reaction between **1** and PyHOTf suggested that other species may form prior to **1H**<sup>+</sup> in the protonation of **1**, meaning the BDE<sub>N-H</sub> in **1H**<sup>+</sup> may not be a driver for this reaction. Nonetheless, the calculated BDE<sub>N-H</sub> value is consistent with the observed reactivity patterns, where 4-X-2,6-DTBP substrates with relatively strong O-H bonds did not react with **2** (e.g., X = CN, NO<sub>2</sub>: BDE<sub>O-H</sub> > 84 kcal/mol) whereas those with BDE<sub>O-H</sub> < 84 kcal/mol did react with **2** (Table 1), demonstrating that thermodynamically the reaction with substrates with strong O-H bonds may not be favorable.

Carboxamidate complex **2** has thus been shown to be capable of PCET oxidation, and the carboxamidate donor group is readily protonated resulting in an amide complex (Scheme 2). We conclude, on the basis of the observation that

#### Scheme 2. Ligand Acid/Base Noninnocence in a 2,6-Pyridinedicarboxamidate Complex



**1H**<sup>+</sup> was the product of the PCET oxidation by **2**, that protonation of the carboxamidate N-atom results in decoordination and rotation around the C<sub>ketone</sub>-N bond. During the PCET reaction, the Ni<sup>III</sup> ion acted as an electron acceptor furnishing Ni<sup>II</sup>. We believe our results provide some insight to recent studies by Fukuzumi and co-workers and Garcia-Bosch and co-workers where carboxamidate complexes have been found to, somewhat unexpectedly, mediate PCET oxidations.<sup>31,32</sup> We postulate that in these cases the carboxamidate ligand could be acting as a H<sup>+</sup>-acceptor (as predicted by Garcia-Bosch using computational methods).

#### CONCLUSION

A coordinatively saturated Ni<sup>III</sup>-carboxamidate complex (**2**) was synthesized and characterized. **2** reacted with phenols with weak O-H bonds but not with hydrocarbons in contrast to analogous [Ni<sup>III</sup>(X)(L)]. **2** reacted with phenols giving rate constants 3–30 times lower than analogous complexes. Thus,

**2** was thermodynamically and kinetically less reactive than analogous complexes with ancillary proton acceptors. Analysis of the kinetics of the reaction with a series of *para*-substituted 2,6-di-*tert*-butylphenol substrates showed that the reaction likely proceeded through a nonconcerted or partially concerted PCET mechanism. It appeared that ET was not exclusively rate limiting, with ET and PT demonstrating similar rates. The supporting carboxamidate ligand was found to be acid–base noninnocent and thus capable of acting as a H<sup>+</sup>-acceptor (forming complex **1H**<sup>+</sup>). Indeed, we demonstrated that the complex remained intact through a full cycle of oxidation of **1** to **2**, PCET by **2** to yield **1H**<sup>+</sup>, and deprotonation of **1H**<sup>+</sup> to yield **1** followed by reoxidation of **1** to yield **2**. The N–H bond dissociation enthalpy of the protonated amide in **1H**<sup>+</sup> was determined to be 84 kcal/mol, and **2** was only capable of oxidizing substrates with O–H bond dissociation enthalpies less than 84 kcal/mol. Our results demonstrate that a carboxamidate ligand can be acid/base noninnocent in PCET oxidation chemistry.

## ■ ASSOCIATED CONTENT

### ● Supporting Information

The Supporting Information is available free of charge on the ACS Publications website at DOI: 10.1021/acs.inorgchem.9b00055.

Physical methods; synthesis methods; reactivity protocols and results; acid/base studies; further EPR analysis; X-ray crystallography data (PDF)

### Accession Codes

CCDC 1850648 and 1885722 contain the supplementary crystallographic data for this paper. These data can be obtained free of charge via [www.ccdc.cam.ac.uk/data\\_request/cif](http://www.ccdc.cam.ac.uk/data_request/cif), or by emailing [data\\_request@ccdc.cam.ac.uk](mailto:data_request@ccdc.cam.ac.uk), or by contacting The Cambridge Crystallographic Data Centre, 12 Union Road, Cambridge CB2 1EZ, UK; fax: +44 1223 336033.

## ■ AUTHOR INFORMATION

### Corresponding Author

\*E-mail: [aidan.mcdonald@tcd.ie](mailto:aidan.mcdonald@tcd.ie).

### ORCID

Aidan R. McDonald: 0000-0002-8930-3256

### Author Contributions

‡C.McM. and P.M. contributed equally.

### Notes

The authors declare no competing financial interest.

## ■ ACKNOWLEDGMENTS

This publication has emanated from research supported by the European Union (ERC-2015-STG-678202). Research in the McDonald lab is supported in part by a research grant from Science Foundation Ireland (SFI/15/RS-URF/3307). We are grateful to Prof. Robert Barkley for training on and use of an EPR spectrometer.

## ■ REFERENCES

- (1) Sheldon, R. A.; Kochi, J. K. *Metal-Catalyzed Oxidation of Organic Compounds*; Academic: New York, 1981.
- (2) Arakawa, H.; Aresta, M.; Armor, J. N.; Barteau, M. A.; Beckman, E. J.; Bell, A. T.; Bercaw, J. E.; Creutz, C.; Dinjus, E.; Dixon, D. A.; Domen, K.; DuBois, D. L.; Eckert, J.; Fujita, E.; Gibson, D. H.; Goddard, W. A.; Goodman, D. W.; Keller, J.; Kubas, G. J.; Kung, H. H.; Lyons, J. E.; Manzer, L. E.; Marks, T. J.; Morokuma, K.; Nicholas,

K. M.; Periana, R.; Que, L.; Rostrup-Nielson, J.; Sachtler, W. M. H.; Schmidt, L. D.; Sen, A.; Somorjai, G. A.; Stair, P. C.; Stults, B. R.; Tumas, W. *Catalysis Research of Relevance to Carbon Management: Progress, Challenges, and Opportunities*. *Chem. Rev.* **2001**, *101* (4), 953–996.

(3) Labinger, J. A.; Bercaw, J. E. Understanding and exploiting C–H bond activation. *Nature* **2002**, *417*, 507.

(4) Que, L., Jr.; Tolman, W. B. Biologically inspired oxidation catalysis. *Nature* **2008**, *455*, 333–340.

(5) Crabtree, R. H. Introduction to Selective Functionalization of C–H Bonds. *Chem. Rev.* **2010**, *110* (2), 575–575a.

(6) Bordeaux, M.; Galarneau, A.; Drone, J. Catalytic, Mild, and Selective Oxyfunctionalization of Linear Alkanes: Current Challenges. *Angew. Chem., Int. Ed.* **2012**, *51* (43), 10712–10723.

(7) Garcia-Bosch, I.; Prat, I.; Ribas, X.; Costas, M. In *Bioinspired oxidations catalyzed by nonheme iron and manganese complexes*; Wiley-VCH Verlag GmbH & Co. KGaA: 2012; pp 27–46.

(8) Costas, M.; Mehn, M. P.; Jensen, M. P.; Que, L., Jr. Oxygen Activation at Mononuclear Nonheme Iron: Enzymes, Intermediates, and Models. *Chem. Rev.* **2004**, *104*, 939–986.

(9) Groves, J. T. Models and Mechanisms of Cytochrome P450 Action. In *Cytochrome P450: Structure, Mechanism, and Biochemistry*, 3rd ed.; Ortiz de Montellano, P. R., Ed.; Kluwer Academic/Plenum Publishers: New York, 2005; pp 1–43.

(10) McDonald, A. R.; Que, L., Jr. High-valent nonheme iron-oxo complexes: Synthesis, structure, and spectroscopy. *Coord. Chem. Rev.* **2013**, *257* (2), 414–428.

(11) Solomon, E. I.; Heppner, D. E.; Johnston, E. M.; Ginsbach, J. W.; Cirera, J.; Qayyum, M.; Kieber-Emmons, M. T.; Kjaergaard, C. H.; Hadt, R. G.; Tian, L. Copper Active Sites in Biology. *Chem. Rev.* **2014**, *114*, 3659.

(12) Elwell, C. E.; Gagnon, N. L.; Neisen, B. D.; Dhar, D.; Spaeth, A. D.; Yee, G. M.; Tolman, W. B. Copper–Oxygen Complexes Revisited: Structures, Spectroscopy, and Reactivity. *Chem. Rev.* **2017**, *117* (3), 2059–2107.

(13) Tshuva, E. Y.; Lippard, S. J. Synthetic Models for Non-Heme Carboxylate-Bridged Diiron Metalloproteins: Strategies and Tactics. *Chem. Rev.* **2004**, *104* (2), 987–1012.

(14) Bartos, M. J.; Gordon-Wylie, S. W.; Fox, B. G.; James Wright, L.; Weintraub, S. T.; Kauffmann, K. E.; Munck, E.; Kostka, K. L.; Uffelman, E. S.; Rickard, C. E. F.; Noon, K. R.; Collins, T. J. Designing ligands to achieve robust oxidation catalysts. Iron based systems. *Coord. Chem. Rev.* **1998**, *174*, 361–390.

(15) Popescu, D.-L.; Chanda, A.; Stadler, M.; de Oliveira, F. T.; Ryabov, A. D.; Münck, E.; Bominaar, E. L.; Collins, T. J. High-valent first-row transition-metal complexes of tetraamido (4N) and diamidodialkoxido or diamidophenolato (2N/2O) ligands: Synthesis, structure, and magnetochemistry. *Coord. Chem. Rev.* **2008**, *252* (18–20), 2050–2071.

(16) Borovik, A. S. Bioinspired hydrogen bond motifs in ligand design: the role of noncovalent interactions in metal ion mediated activation of dioxygen. *Acc. Chem. Res.* **2005**, *38*, 54–61.

(17) Stone, K. L.; Borovik, A. S. Lessons from nature: unraveling biological C–H bond activation. *Curr. Opin. Chem. Biol.* **2009**, *13*, 114–118.

(18) Borovik, A. S. Role of metal-oxo complexes in the cleavage of C–H bonds. *Chem. Soc. Rev.* **2011**, *40*, 1870–4.

(19) Lacy, D. C.; Mukherjee, J.; Lucas, R. L.; Day, V. W.; Borovik, A. S. Metal complexes with varying intramolecular hydrogen bonding networks. *Polyhedron* **2013**, *52*, 261–267.

(20) Donoghue, P. J.; Tehranchi, J.; Cramer, C. J.; Sarangi, R.; Solomon, E. I.; Tolman, W. B. Rapid C–H bond activation by a monocopper(III)-hydroxide complex. *J. Am. Chem. Soc.* **2011**, *133*, 17602–17605.

(21) Halvagar, M. R.; Solntsev, P. V.; Lim, H.; Hedman, B.; Hodgson, K. O.; Solomon, E. I.; Cramer, C. J.; Tolman, W. B. Hydroxo-Bridged Dicopper(II,III) and -(III,III) Complexes: Models for Putative Intermediates in Oxidation Catalysis. *J. Am. Chem. Soc.* **2014**, *136*, 7269–7272.

- (22) Gagnon, N.; Tolman, W. B.  $[\text{CuO}]^+$  and  $[\text{CuOH}]^{2+}$  complexes: intermediates in oxidation catalysis? *Acc. Chem. Res.* **2015**, *48* (7), 2126–2131.
- (23) Patra, A. K.; Mukherjee, R. Bivalent, Trivalent, and Tetravalent Nickel Complexes with a Common Tridentate Deprotonated Pyridine Bis-Amide Ligand. Molecular Structures of Nickel(II) and Nickel(IV) and Redox Activity. *Inorg. Chem.* **1999**, *38*, 1388–1393.
- (24) Pirovano, P.; Farquhar, E. R.; Swart, M.; Fitzpatrick, A. J.; Morgan, G. G.; McDonald, A. R. Characterization and Reactivity of a Terminal Nickel(III)–Oxygen Adduct. *Chem. - Eur. J.* **2015**, *21*, 3785–3790.
- (25) Corona, T.; Pfaff, F. F.; Acuña-Parés, F.; Draksharapu, A.; Whiteoak, C. J.; Martin-Diaconescu, V.; Lloret-Fillol, J.; Browne, W. R.; Ray, K.; Company, A. Reactivity of a Nickel(II) Bis(amidate) Complex with meta-Chloroperbenzoic Acid: Formation of a Potent Oxidizing Species. *Chem. - Eur. J.* **2015**, *21* (42), 15029–15038.
- (26) Pirovano, P.; Farquhar, E. R.; Swart, M.; McDonald, A. R. Tuning the Reactivity of Terminal Nickel(III)–Oxygen Adducts for C–H Bond Activation. *J. Am. Chem. Soc.* **2016**, *138* (43), 14362–14370.
- (27) Corona, T.; Draksharapu, A.; Padamati, S. K.; Gamba, I.; Martin-Diaconescu, V.; Acuña-Parés, F.; Browne, W. R.; Company, A. Rapid Hydrogen and Oxygen Atom Transfer by a High-Valent Nickel–Oxygen Species. *J. Am. Chem. Soc.* **2016**, *138* (39), 12987–12996.
- (28) Mondal, P.; Pirovano, P.; Das, A.; Farquhar, E. R.; McDonald, A. R. Hydrogen Atom Transfer by a High-Valent Nickel-Chloride Complex. *J. Am. Chem. Soc.* **2018**, *140* (5), 1834–1841.
- (29) Pirovano, P.; Berry, A. R.; Swart, M.; McDonald, A. R. Indirect evidence for a  $\text{Ni}^{\text{III}}$ -oxyl oxidant in the reaction of a  $\text{Ni}^{\text{II}}$  complex with peracid. *Dalton Trans* **2018**, *47* (1), 246–250.
- (30) Pirovano, P.; Twamley, B.; McDonald, A. R. Modulation of Nickel Pyridinedicarboxamidate Complexes to Explore the Properties of High-valent Oxidants. *Chem. - Eur. J.* **2018**, *24* (20), 5238–5245.
- (31) Sankaralingam, M.; Lee, Y.-M.; Karmalkar, D. G.; Nam, W.; Fukuzumi, S. A Mononuclear Non-heme Manganese(III)–Aqua Complex as a New Active Oxidant in Hydrogen Atom Transfer Reactions. *J. Am. Chem. Soc.* **2018**, *140* (40), 12695–12699.
- (32) Rajabimoghadam, K.; Darwish, Y.; Bashir, U.; Pitman, D.; Eichelberger, S.; Siegler, M. A.; Swart, M.; Garcia-Bosch, I. Catalytic Aerobic Oxidation of Alcohols by Copper Complexes Bearing Redox-Active Ligands with Tunable H-Bonding Groups. *J. Am. Chem. Soc.* **2018**, *140* (48), 16625–16634.
- (33) Huynh, M. H. V.; Meyer, T. J. Proton-Coupled Electron Transfer. *Chem. Rev.* **2007**, *107* (11), 5004–5064.
- (34) Warren, J. J.; Tronic, T. A.; Mayer, J. M. Thermochemistry of proton-coupled electron transfer reagents and its implications. *Chem. Rev.* **2010**, *110* (12), 6961–7001.
- (35) Hammes-Schiffer, S.; Stuchebrukhov, A. A. Theory of Coupled Electron and Proton Transfer Reactions. *Chem. Rev.* **2010**, *110* (12), 6939–6960.
- (36) Mayer, J. M. Understanding hydrogen atom transfer: from bond strengths to Marcus theory. *Acc. Chem. Res.* **2011**, *44*, 36–46.
- (37) Rosenkoetter, K. E.; Wojnar, M. K.; Charette, B. J.; Ziller, J. W.; Heyduk, A. F. Hydrogen-Atom Noninnocence of a Tridentate [SNS] Pincer Ligand. *Inorg. Chem.* **2018**, *57* (16), 9728–9737.
- (38) Belle, C.; Bougault, C.; Averbuch, M.-T.; Durif, A.; Pierre, J.-L.; Latour, J.-M.; Le Pape, L. Paramagnetic NMR Investigations of High-Spin Nickel(II) Complexes. Controlled Synthesis, Structural, Electronic, and Magnetic Properties of Dinuclear vs Mononuclear Species. *J. Am. Chem. Soc.* **2001**, *123* (33), 8053–8066.
- (39) Barefield, E. K.; Busch, D. H.; Nelson, S. M. Iron, cobalt, and nickel complexes having anomalous magnetic moments. *Q. Rev., Chem. Soc.* **1968**, *22* (4), 457–498.
- (40) Kruger, H. J.; Peng, G.; Holm, R. H. Low-Potential Nickel(III,II) Complexes - New Systems Based on Tetradentate Amidate Thiolate Ligands and the Influence of Ligand Structure on Potentials in Relation to the Nickel Site in  $[\text{NiFe}]$ -Hydrogenases. *Inorg. Chem.* **1991**, *30* (4), 734–742.
- (41) Corona, T.; Company, A. Spectroscopically Characterized Synthetic Mononuclear Nickel–Oxygen Species. *Chem. - Eur. J.* **2016**, *22* (38), 13422–13429.
- (42) Haines, R. I.; McAuley, A. Synthesis and reactions of nickel(III) complexes. *Coord. Chem. Rev.* **1981**, *39*, 77–119.
- (43) Collins, T. J.; Nichols, T. R.; Uffelman, E. S. A square-planar nickel(III) complex of an innocent ligand system. *J. Am. Chem. Soc.* **1991**, *113* (12), 4708–9.
- (44) Stuart, J. N.; Goerges, A. L.; Zaleski, J. M. Characterization of the Ni(III) Intermediate in the Reaction of (1,4,8,11-Tetraazacyclotetradecane)nickel(II) Perchlorate with  $\text{KHSO}_5$ : Implications to the Mechanism of Oxidative DNA Modification. *Inorg. Chem.* **2000**, *39*, 5976–5984.
- (45) Pirovano, P.; McDonald, A. R. Synthetic High-Valent M–O–X Oxidants. *Eur. J. Inorg. Chem.* **2018**, *2018* (5), 547–560.
- (46) Brigati, G.; Lucarini, M.; Mugnaini, V.; Pedulli, G. F. Determination of the Substituent Effect on the O–H Bond Dissociation Enthalpies of Phenolic Antioxidants by the EPR Radical Equilibration Technique. *J. Org. Chem.* **2002**, *67* (14), 4828–4832.
- (47) Lee, J. Y.; Peterson, R. L.; Ohkubo, K.; Garcia-Bosch, I.; Himes, R. a.; Woertink, J.; Moore, C. D.; Solomon, E. I.; Fukuzumi, S.; Karlin, K. D. Mechanistic insights into the oxidation of substituted phenols via hydrogen atom abstraction by a cupric-superoxo complex. *J. Am. Chem. Soc.* **2014**, *136*, 9925–9937.
- (48) Kundu, S.; Miceli, E.; Farquhar, E. R.; Ray, K. Mechanism of phenol oxidation by heterodinuclear Ni Cu bis( $\mu$ -oxo) complexes involving nucleophilic oxo groups. *Dalton Trans* **2014**, *43*, 4264–4267.
- (49) Sastri, C. V.; Lee, J.; Oh, K.; Lee, Y. J.; Lee, J.; Jackson, T. A.; Ray, K.; Hirao, H.; Shin, W.; Halfen, J. A.; Kim, J.; Que, L., Jr.; Shaik, S.; Nam, W. Axial ligand tuning of a nonheme iron(IV)–oxo unit for hydrogen atom abstraction. *Proc. Natl. Acad. Sci. U. S. A.* **2007**, *104*, 19181–19186.
- (50) Yiu, D. T. Y.; Lee, M. F. W.; Lam, W. W. Y.; Lau, T.-C. Kinetics and Mechanisms of the Oxidation of Phenols by a trans-Dioxoruthenium(VI) Complex. *Inorg. Chem.* **2003**, *42* (4), 1225–1232.
- (51) Lansky, D. E.; Goldberg, D. P. Hydrogen Atom Abstraction by a High-Valent Manganese(V)–Oxo Corrolazine. *Inorg. Chem.* **2006**, *45* (13), 5119–5125.
- (52) Markle, T. F.; Darcy, J. W.; Mayer, J. M. A new strategy to efficiently cleave and form C–H bonds using proton-coupled electron transfer. *Sci. Adv.* **2018**, *4* (7), No. eaat5776.
- (53) Darcy, J. W.; Koronkiewicz, B.; Parada, G. A.; Mayer, J. M. A Continuum of Proton-Coupled Electron Transfer Reactivity. *Acc. Chem. Res.* **2018**, *51* (10), 2391–2399.
- (54) Ram, M. S.; Hupp, J. T. Linear free energy relations for multielectron transfer kinetics: a brief look at the Bronsted/Tafel analogy. *J. Phys. Chem.* **1990**, *94* (6), 2378–2380.
- (55) Weatherly, S. C.; Yang, I. V.; Thorp, H. H. Proton-Coupled Electron Transfer in Duplex DNA: Driving Force Dependence and Isotope Effects on Electrocatalytic Oxidation of Guanine. *J. Am. Chem. Soc.* **2001**, *123* (6), 1236–1237.
- (56) Osako, T.; Ohkubo, K.; Taki, M.; Tachi, Y.; Fukuzumi, S.; Itoh, S. Oxidation Mechanism of Phenols by Dicopper–Dioxygen ( $\text{Cu}_2/\text{O}_2$ ) Complexes. *J. Am. Chem. Soc.* **2003**, *125* (36), 11027–11033.
- (57) Garcia-Bosch, I.; Cowley, R. E.; Díaz, D. E.; Peterson, R. L.; Solomon, E. I.; Karlin, K. D. Substrate and Lewis Acid Coordination Promote O–O Bond Cleavage of an Unreactive  $\text{L}_2\text{Cu}^{\text{II}}_2(\text{O}_2^{2-})$  Species to Form  $\text{L}_2\text{Cu}^{\text{III}}_2(\text{O})_2$  Cores with Enhanced Oxidative Reactivity. *J. Am. Chem. Soc.* **2017**, *139* (8), 3186–3195.
- (58) Guttenplan, J. B.; Cohen, S. G. Triplet energies, reduction potentials, and ionization potentials in carbonyl-donor partial charge-transfer interactions. *J. Am. Chem. Soc.* **1972**, *94* (11), 4040–4042.